Two-Color, Laser Excitation Improves Temporal Resolution for Detecting the Dynamic, Plasmonic Coupling between Metallic Nanoparticles

ARTICLE *in* ANALYTICAL CHEMISTRY · APRIL 2013

Impact Factor: 5.64 · DOI: 10.1021/ac4004453 · Source: PubMed

2 AUTHORS, INCLUDING:

Troy A Lionberger
University of California, Berkeley
34 PUBLICATIONS **72** CITATIONS

analytical chemistry

Article

pubs.acs.org/ac

Two-Color, Laser Excitation Improves Temporal Resolution for Detecting the Dynamic, Plasmonic Coupling between Metallic Nanoparticles

Diane M. Wiener*[,∥,†] and Troy A. Lionberger*[,∥,⊥,¶]

[∥]Department of Mechanical Engineering and [⊥]Cellular and Molecular Biology Program, University of Michigan, Ann Arbor, Michigan 48109, United States

Supporting Information

ABSTRACT: The ability of two, scattering gold nanoparticles (GNPs) to plasmonically couple in a manner that is dependent on the interparticle separation has been exploited to measure nanometer-level displacements. However, despite broad applicability to monitoring biophysical dynamics, the long time scales (<5 Hz) with which plasmonic coupling are typically measured are not suitable for many dynamic molecular processes, generally occurring over several milliseconds. Here, we introduce a new technique intended to overcome this technical limitation: ratiometric analysis using monochromatic, evanescent darkfield illumination (RAMEDI). As a proof-of-principle, we monitored dynamic, plasmonic coupling arising from the binding of single biotin- and neutravidin-GNPs with a temporal resolution of 38 ms. We also show that the observable bandwidth is extendable to faster time scales by demonstrating that RAMEDI is capable of achieving a signal-to-noise ratio greater than 20 from individual GNPs observed with 200 Hz bandwidth.

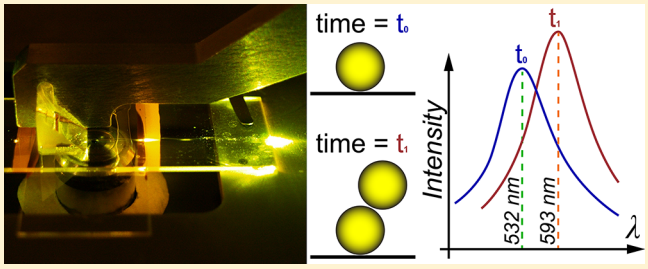

A broad number of fields are currently interested in probing complex nanoscale, biomolecular phenomena. The pressing need to characterize molecular interactions, nanomaterials, and nanoscale devices has fueled the development of techniques capable of accurately measuring nanometer displacements and fast dynamics of time-dependent processes. Progress in these areas has been limited by the lack of suitable techniques capable of characterizing systems meeting three desired specifications: (1) subnanometer spatial resolution; (2) a wide, dynamic distance range exceeding 10 nm; and (3) a temporal resolution on the order of micro- to a few milliseconds. Currently, the most widely used optical technique for dynamic distance measurement with a resolution below the diffraction limit of light is fluorescence resonance energy transfer (FRET). However, FRET suffers from the inherent trade-off between fluorescence intensity (temporal resolution) and photostability (duration of the observation).[1,2] In FRET, as with any fluorescence-based observation, the balance between temporal resolution and observational lifetime is intrinsically limited by the photophysical properties of fluorescent molecules (e.g., photobleaching and blinking).[2] Next generation alternatives to FRET will likely involve an optical signal that does not involve fluorescence. The distance-dependent behavior of light scattering from pairs of metallic nanoparticles is a well-suited alternative capable of overcoming the limitations of FRET and motivates the current work.

Metal nanoparticles (and in particular, gold nanoparticles) are in many ways ideal molecular probes. They are extremely photostable, can be covalently conjugated to biomolecules through gold−thiol chemistry, are biologically inert, and scatter light efficiently.[3] The scattering intensity can be amplified when metallic nanoparticles are illuminated with light at a particular resonance wavelength, λ_{PR}. Here, scattering is enhanced due to the resonant excitation of conduction electrons at the interfaces of metallic and dielectric materials. Surface plasmons are excited by the electric field of the incident electromagnetic radiation, which induces an in-phase dipole of the conduction electrons. A surface restoring force created by illumination at the resonance frequency compensates for the dipole, causing the electrons to oscillate coherently.[3−8] Gold nanoparticles (GNPs) are commonly used because they exhibit sharp plasmon resonance peaks in the visible spectrum, making them ideal for applications using visible light microscopy. As such, they have been widely used in fields ranging from photonics, materials science, electronics, and energetics to biosensing, biotechnology, and single-molecule biophysics.[5,9−13]

The plasmon resonance wavelength for metallic nanoparticles strongly depends on many factors, including nanoparticle composition, size, shape (aspect ratio), and the refractive index of the surrounding medium.[5,9−13] Additionally, the plasmon resonance behavior of GNPs depends on the proximity of neighboring nanoparticles through a phenomenon known as plasmonic coupling. When two GNPs are brought within ∼2.5 times the diameter of the particles, surface

Received: February 9, 2013
Accepted: April 12, 2013

   dx.doi.org/10.1021/ac4004453 | *Anal. Chem.* XXXX, XXX, XXX−XXX

plasmons generated in each particle couple to a degree that is nonlinearly related to the interparticle distance.[11] As the distance between two GNPs decreases, the free conduction electrons of the nanoparticles couple more strongly, resulting in a shift of λ_{PR} toward longer wavelengths (i.e., red-shifting).[14] By monitoring the red-shifting of λ_{PR} as two GNPs interact, plasmonic coupling has been used to measure the dynamic behavior of biomolecules with nanometer resolution.[11,12,15,16] However, the temporal resolution over which these interactions can be monitored often precludes the application of plasmonic coupling to many biological systems. Motivated by earlier work with plasmonic molecular rulers,[11,12,15,16] we sought to develop a technique that is capable of detecting the plasmonic coupling between GNPs with high temporal resolution.

Previous applications of plasmonic coupling have largely relied on the use of broadband illumination and detailed spectral characterization in an effort to directly find λ_{PR} from the spectrum of light scattered from GNPs.[11,12,17,18] However, there are several important, technical drawbacks in analyzing the scattering spectra of individual GNPs. Light scattered from a single GNP is typically very weak under illumination by broadband light sources, often approaching the reliable detection limit for conventional spectrometers. Owing to the low scattering intensity under these conditions, the exposure time needed to reconstruct the scattering spectrum from a single GNP is on the order of hundreds of milliseconds to minutes.[11,12] Previous methods relying on spectral characterization also depend on the accurate determination of λ_{PR} from a scattering spectrum. However, individual spectra are often very noisy, making accurate determination of λ_{PR} challenging given the typical need to resolve spectral red-shifting of less than 5 nm.[11,12,17,18] In addition, λ_{PR} can only be determined using fitting approaches that depend on assumed behaviors of the spectra as a function of distance, which are also known to vary with the polarization of the illumination, nanoparticle size and shape, and refractive index, among other factors.[5,6,11,13,17−23] Here, we present a method, referred to as ratiometric analysis using monochromatic, evanescent darkfield illumination (RAMEDI), that overcomes many of the limitations of previous techniques by effectively narrowing the excitation wavelengths that are used and increasing the intensity of the illumination. As a proof-of-principle demonstration, we used RAMEDI to monitor the plasmonic coupling originating from the binding of surface-bound biotin-GNPs to neutravidin-conjugated GNPs in solution.

Using RAMEDI, we can follow the dynamic plasmonic coupling between two GNPs with greater than 25 Hz bandwidth. We observe individual GNP scattering intensities better than 100 times the background and demonstrate that the intensity ratio more than doubles upon binding a second GNP. Further, we are able to record the scattering signal from a single GNP at 200 Hz (the fastest acquisition time of our detector), achieving a signal-to-noise ratio above 20. This observation establishes that RAMEDI is, in principle, fully extendable to faster time scales and is currently limited only by the choice of detector and the number of simultaneous observations being made. Finally, we demonstrate that RAMEDI is sensitive to the polarization of the incident light. Using two, orthogonal orientations of linearly polarized excitation, we observe a polarization sensitivity as large as 2.5 times, thus establishing that it is possible to relate the detected signal to the orientation of the interacting particles. Taken together, we contend that these demonstrations mark a needed, technical advance in furthering the use of plasmonic coupling between metallic nanoparticles as a powerful alternative to FRET and other nanoscale measurement techniques.

EXPERIMENTAL SECTION

Experimental Setup. The evanescent darkfield setup (see Supporting Information for details) was mounted on an inverted Zeiss Axiovert 200 microscope. We replaced the conventional microscope stage and objective focusing mechanism with a custom designed, low-drift, flexure stage to minimize thermal and mechanical drift, making it possible to conduct long time-duration, single-molecule experiments in which stability in both focus and stage location are required. The custom stage has less than 200 nm of drift in the x and y directions during the first hour of the observation and no detectable drift in the z (objective focus) position. The majority of the drift is accounted to thermal expansion of the microscope stage. Further, the stage incorporates a commercially available piezoelectric stage (Physik Instrumente, P-541.2CD) for precise nanometer translation (300 μm lateral travel with ±0.4 nm resolution). A 100× Zeiss Achroplan variable-aperture, oil objective (NA 0.7−1.25, set to NA 1.25 in our experiments) collects the scattered light from the microscope. The scattering signal from the two wavelengths are split using a commercial dual-view imaging system (Photometric, DV2 Dual-View) with a dichroic mirror (Chroma, 565dcxr) and imaged with an EMCCD camera (Photometrics, Cascade 512F).

General Preparations. Biotin- and neutravidin-GNPs were purchased from NanoPartz (20-PB-40, 20-PN-40) with a nominal diameter of 40 nm at a concentration of 20 nM. See the Supporting Information for further details regarding conjugation, size distribution, and surface charge.

Biotin-Neutravidin Gold Nanoparticle Binding Experiments. Biotin-neutravidin GNP assays were performed in two parallel steps: (1) passivating the neutravidin-GNPs and (2) preparing a glass assay chamber within which to bind the biotin-GNPs. The neutravidin-GNPs were diluted to 55 pM in a passivation solution composed of 0.5 mg/mL biotin-free casein and 0.5 mg/mL BSA dissolved in T40 buffer (10 mM Tris, pH 7.0−8.0 and 40 mM NaCl). The neutravidin-GNPs are incubated for 30 min at room temperature.

T-shaped assay chambers were constructed with a cleaned 24 mm × 40 mm #1 glass cover slide and a glass slide with #0000 glass shards (nominal thickness 50 μm) in vacuum grease serving as spacers. The biotin-GNPs were diluted to 6 pM in T40 buffer and incubated for 2 min in the chamber. The chamber was washed with T40 buffer, and then, the surface was passivated with 0.1 mg/mL biotin-free casein in T40 buffer for 15 min followed by another 15-min incubation with 0.1 mg/mL BSA supplemented with 0.1 mg/mL biotin-free casein in T40 buffer. We found that the GNPs were stable and disperse in high ionic strength solutions up to 150 mM NaCl and 25 mM $MgCl_2$ after the simple passivation scheme with biotin-free casein and BSA.

Images were recorded of the biotin-GNPs on the surface prior to introducing the neutravidin-GNPs into the assay chamber. Subsequently, images or image series of the time-resolved binding between the neutravidin-GNP to the biotin-GNP were recorded.

Data Analysis. For all of the plasmonic coupling experiments, the intensities of the GNPs were calculated from both channels using ImageJ (NIH). The intensities were back-

dx.doi.org/10.1021/ac4004453 | Anal. Chem. XXXX, XXX, XXX−XXX

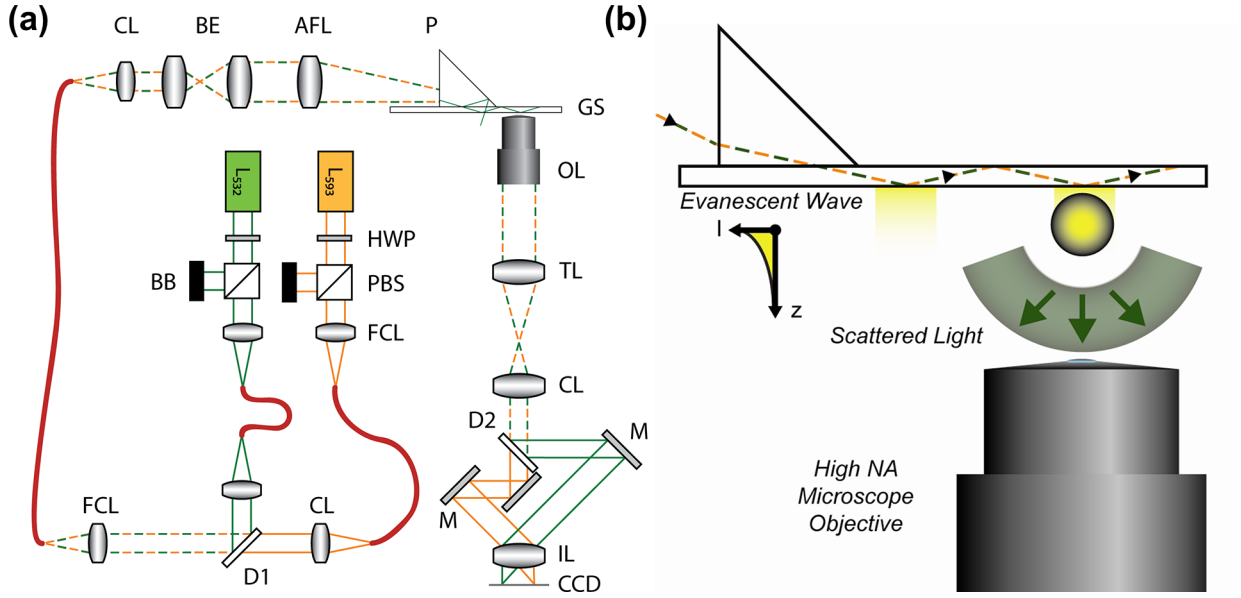

Figure 1. Experimental setup. (a) The experimental schematic, as detailed in the text, couples the intensity from two wavelengths and combines them into a single-mode fiber. An achromatic lens (AFL) focuses the light to a right-angle prism (P) that couples the darkfield illumination into the 1 mm glass slide, wherein it propagates along the slide through total internal reflection. At each reflection within the glass slide, an evanescent field is simultaneously generated with the two illumination wavelengths. The image from the microscope objective is spatially separated with a dichroic mirror and imaged on two regions of a CCD array. (b) An evanescent wave, produced at the glass surface, illuminates only GNPs within ~200 nm depth. Abbreviations: collimation lens (CL), beam expander (BE), achromatic focusing lens (AFL), right-angle prism (P), glass slide (GS), objective lens (OL), tube lens (TL), dichroic mirrors (D1, D2), mirror (M), imaging lens (IL), CCD camera (CCD), fiber coupling lens (FLC), beam block (BB), polarizing beamsplitter (PBS), $\lambda/2$ waveplate (HWP), 532 nm laser (L_{532}), and 593 nm laser (L_{593}).

ground-corrected using the background from the individual wavelength channels. The intensity ratios of the 593 nm background-corrected intensity and the 532 nm background-corrected intensity were calculated with a custom MATLAB (The MathWorks) routine.

RESULTS AND DISCUSSION

Monochromatic Evanescent Darkfield Illumination Enables Observations of GNPs with >200 Hz Bandwidth. In all high-resolution imaging techniques, the time resolution with which a dynamic process can be observed is directly related to the intensity of the observed signal above the background. Consequently, increasing the temporal resolution of an observation requires that we maintain an adequately high signal-to-background ratio (i.e., high intensity optical signals and/or low background). The practical limitations of fluorescence-based methods, such as FRET, may be overcome by instead measuring the scattering response from metallic nanoparticles. The main technical advantage of scattering-based techniques is that arbitrarily high illumination intensities can be used to increase the intensity of the optical signal without photobleaching the sample, but unlike fluorescence-based methods, the background signal is more difficult to reduce because scattering necessarily requires that the same wavelength is used for both illumination and observation. Therefore, optical filters, typically used in fluorescence techniques, cannot be used to chromatically separate the illumination from the desired signal.

All darkfield imaging techniques minimize the background by geometrically separating the path of the illumination from the desired signal. However, even using modern darkfield illumination methods, illumination is transmitted to the entire sample and therefore increases background from scatterers in solution. This background is limiting in cases where high concentrations of scatterers are desired, as is typically the case for many binding assays intended to characterize the interaction between two biomolecules. Another important limitation of conventional darkfield imaging methods, particularly with respect to illuminating nanoscopic metallic particles, is that these techniques typically use broadband, incoherent light sources. Illumination using incoherent light inherently limits the power density transmitted to a nanoparticle sample if only particular wavelengths of light (e.g., λ_{PR}) are desired.[16,24]

To address the limited power density capable of being transmitted to a scattering sample using conventional darkfield techniques, we designed an experimental setup capable of performing darkfield illumination using the evanescent field established through prism-based, total internal reflection with laser illumination. The resulting monochromatic evanescent darkfield illumination (MEDI) isolates the excitation completely from the objective lens used to collect the light, minimizing background and making it possible to efficiently observe light scattering from GNPs. In addition, MEDI limits the region of excitation to a depth on the order of 100−200 nm. This further rejects the background signal due to GNPs that remain free in solution. Using MEDI, the power density at the sample can simply be increased through focusing the monochromatic light (limited only by the diffraction limit) to enhance the scattering signal from the GNPs, thereby enabling higher temporal resolution. MEDI also increases the collection efficiency of the scattered light since high NA objective lenses can be used (not typically possible in conventional darkfield microscopy setups). Finally, back-reflections of the excitation source are excluded by propagating the totally internally reflecting light though the glass slide of the assay chamber, making the implementation of prism-based MEDI technically more straightforward than objective-type total internal

dx.doi.org/10.1021/ac4004453 | Anal. Chem. XXXX, XXX, XXX−XXX

reflection designs.[25,26] Figure 1 details the experimental configuration of our prism-based, MEDI setup (see the Supporting Information for additional details).

As discussed previously, determining λ_{PR} using spectral characterization and broadband illumination is susceptible to error that is inherent to signal-limited, noisy spectra. Building upon the first implementations of ratiometric detection schemes,[23,27] we attempted to address these technical issues by monitoring only two particular scattering wavelengths in lieu of spectral analysis using broadband illumination. However, in the previous iterations of ratiometric detection, nanoparticles were sequentially illuminated by two bandpasses of broadband excitation, selected using a filter wheel, and the intensity ratio was calculated from the collected images. On the other hand, our technique, RAMEDI, enables the simultaneous acquisition of the scattering intensity using two sampling wavelengths. These two signals are then spatially separated between two halves of a CCD array using a dual view imaging system (Figure 1). Our instrument is a technically straightforward, though significant, advance building upon previous ratiometric analysis techniques.[23,27]

For our proof-of-principle demonstrations using RAMEDI, we have chosen to use GNPs 40 nm in diameter observed with 532 and 593 nm laser illumination. The intensity ratio is calculated from the scattering signal from the two sampling wavelengths, making their selection an important design consideration given the diameter of the GNP used in the assay. Our choice to use 40 nm GNPs was motivated by previously published spectral information for both individual particles and GNP dimers at varying interparticle separations.[11] From the experimental spectra reported by Reinhard et al.,[11] we calculated the theoretical intensity ratio as a function of interparticle separation for various sampling wavelengths, thus allowing us to optimize our choice of wavelengths for a particular application (see Supporting Information for details). As shown in Table 1, when the edge-to-edge separation of two

Table 1. Theoretical Predictions of Ratiometric Response[a]

DNA tether length [bp]	particle separation [nm]	peak wavelength [nm]	593 nm/532 nm ratio
67	29.3	563	0.0349
20	14.7	567.8	1.437

[a]The ratiometric response for selected sampling wavelengths is compared to the peak resonance wavelengths. The intensity ratio was calculated using the experimental spectra collected at several particle separations published by Reinhard et al.[11]

40 nm GNPs decreases by roughly 2-fold, λ_{PR} changes by less than 1%. However, the ratio of scattering intensity for the two wavelengths selected for our measurements (532 and 593 nm) increases by more than 40 times. Accordingly, RAMEDI significantly enhances sensitivity in detecting changes in interparticle separations over previous methods relying on the detection of λ_{PR} from spectral analysis of light scattered from GNPs.

Accurately measuring the ratiometric response from a dynamic interaction between GNPs requires that we collect the light scattered at both sampling wavelengths with a detector that has sufficient temporal resolution for the target application. We chose to image the scattered light onto an EMCCD camera so that many GNPs may be observed within a single field of view. Using the full image array of the CCD camera, it is possible to observe individual GNPs with 38 ms temporal resolution and a signal-to-background ratio greater than 100. When the region of interest is reduced to the size of a diffraction-limited spot, we can image the scattering from a 40 nm GNP with the fastest temporal resolution of our camera (5 ms) and a signal-to-background ratio of more than 20. Thus, the temporal resolution is not signal-limited using an EMCCD camera, and time resolutions appropriate for studying many biomolecular phenomena are possible.

It should be noted that, whereas in the current implementation, RAMEDI has achieved a temporal resolution that is comparable to previously reported techniques,[16,23] our observations are currently limited only by the acquisition time of our EMCCD camera. Given the high signal-to-background ratio we observe, however, future implementations using other detectors (e.g., CMOS CCD arrays, avalanche photodiodes, photomultiplier tubes) are expected to further improve the observable bandwidth of the technique. In contrast to incoherent, broadband illumination methods,[23,27] the increase in scattering brightness above background (and hence temporal resolution) achieved through tighter focusing of the illumination is limited only by diffraction. Therefore, given that laser illumination concentrates optical power at particular sampling wavelengths and the power density at the sample plane is limited only by diffraction, these data suggest that RAMEDI is capable of monitoring dynamic, plasmonic coupling between metallic nanoparticles with a temporal resolution that is practically limited by the technical specifications of a chosen detector.

Changes in the Intensity Ratio That Accompany the Plasmonic Coupling between Two GNPs Can Be Used to Detect Protein Binding. To demonstrate that RAMEDI can be applied to studying biological systems, we performed a proof-of-principle assay monitoring the binding of neutravidin-GNPs to surface-bound biotin-GNPs. Before conducting the binding assay, we performed a baseline observation of biotin-GNPs used in this study by binding a sample to a glass surface and then measuring the intensity ratio (I_{593}/I_{532}) of all particles over several fields of view. The intensity ratios from 88 biotin-GNPs were measured with a mean intensity ratio of 0.938 ± 0.14 (mean ± S.D.). The variations in the scattering ratios between individual particles are attributed to the known dependence of λ_{PR} on the particle size/shape distributions and the local refractive index variations owing to the protein and polymer coatings on our particles (see Supporting Information), as has been noted in the literature.[5,11,23]

Following our baseline observation of the biotin-GNP population, we next sought to determine the expected maximal change in intensity ratio that would accompany binding of a freely diffusing neutravidin-GNP to the surface-bound biotin-GNP (see the Supporting Information for details of the biotin-streptavidin interaction). First, we imaged surface-bound biotin-GNPs and calculated the initial intensity ratio, verifying consistency with our baseline observation. Then, we incubated these biotin-GNPs with neutravidin-GNPs for 5 min, reimaged the same field of view of GNPs, and compared the ratio of the scattered light before and after the incubation. Before the neutravidin-GNPs were incubated, the surface-bound biotin-GNPs preferentially scatter the 532 nm wavelength. After the incubation, binding of a neutravidin-GNP to a biotin-GNP is accompanied by both an increase in the total intensity and a change in the intensity ratio (Figure 2). We observe that the scattering intensity ratio of a surface-bound biotin-GNP

dx.doi.org/10.1021/ac4004453 | Anal. Chem. XXXX, XXX, XXX−XXX

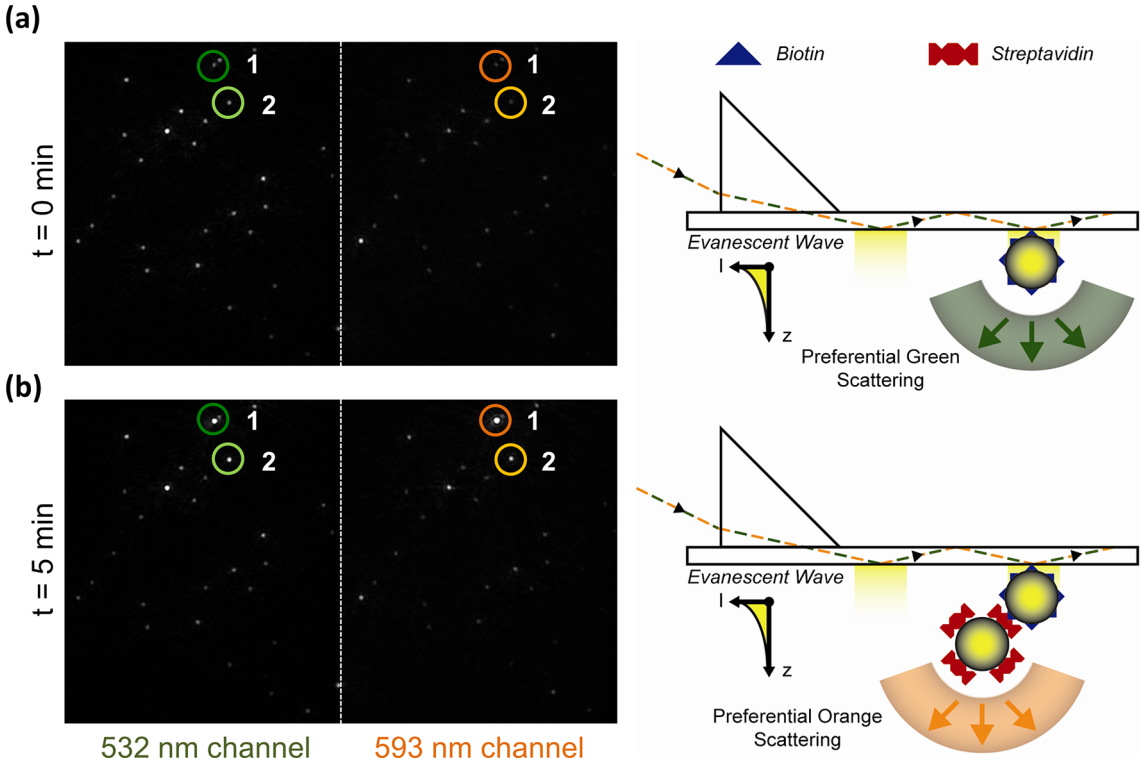

Figure 2. Observing gold nanoparticle scattering and plasmonic coupling using RAMEDI. The scattering signal is collected from the two wavelengths of excitation (532 nm, left side of image, and 593 nm, right side of image) in the same image. (a) Surface-bound biotin-GNPs are imaged with the dual view imaging system under dual wavelength excitation before incubation with neutravidin-GNPs. (b) The same field of view is imaged after a 5 min incubation with neutravidin-GNPs. Binding between two GNPs is clearly observed by a total intensity increase and an increase in the intensity ratio for the two gold nanoparticle pairs (dark and light circles) indicated in the images. A clear advantage of the technique is its ability to continuously monitor several gold nanoparticle pairs simultaneously. Control experiments verify that the binding reactions are specific biotin-neutravidin conjugations.

increases by a factor of 1.5 to 2 times after binding of a neutravidin-GNP. Measuring the intensity ratios of non-interacting biotin-GNPs served as internal controls within all of the binding assays to discern between spherical monomers and larger aggregates or anisotropic particles. While it is possible to limit our observations to the specific surface-bound biotin-GNPs with ratios consistent with 40 nm diameter monomers, there is no control over the size and shape of the neutravidin-GNP that binds. However, when only two distinct states of the plasmonic response are necessary to distinguish (e.g., discriminating GNP binding), heterogeneities in GNP size and shape distributions are expected to have a negligible impact on the experimental confidence of identifying binding events. Applications requiring the measurement of precise interparticle separations naturally require higher levels of stringency with respect to the GNP populations since the nanoparticle size and shape will have direct implications on the plasmonic response as a function of interparticle distance.

To verify that the observed plasmonic interactions were arising from the specific binding of the biotin to neutravidin, we performed two negative controls. In the first control experiment, surface-bound biotin-GNPs were incubated with freely diffusing biotin-GNPs. After 30 min, no change in either the intensity ratio or total intensity of surface-bound GNPs was observed, consistent with our expectation that no binding should occur. Moreover, no additional particles bound to the surface, confirming that our passivation method limits non-specific binding of GNPs to the surface. As a second negative control, we preincubated neutravidin-GNPs with a 10 000-fold molar excess of free biotin in order to saturate and occupy all available neutravidin binding sites. The off-rate of biotin from neutravidin has been measured to have a half-life of ~3 h; thus, with such a high excess of free biotin in solution, the neutravidin-GNPs should remain free in solution and unavailable to bind to the surface-bound biotin-GNPs.[28] Again, no binding was observed after an incubation of 30 min. For both control experiments, the observed particle intensity ratio distributions over several fields of view were statistically indistinguishable before and after the incubations, confirming that no plasmonic coupling interactions occurred.

Dynamic Binding Interactions between GNPs Can Be Observed with 38 ms Resolution. Many molecular processes in biological systems occur on the millisecond time scale. Therefore, characterizing the dynamics of short-lived biological activities often requires observations to be made on the millisecond to submillisecond time scale. Despite significant recognition of plasmonic interactions by GNPs to be a viable tool in studying dynamic, molecular phenomena, a method has yet to emerge that can clearly be extended to observations on the necessary time scales. We sought to evaluate the technical feasibility of RAMEDI to extend to faster temporal resolutions using the biotin-neutravidin binding assay as a model system for short-lived biological processes. While observing surface-bound biotin-GNPs, we introduced neutravidin-GNPs into the assay chamber by capillary action and allowed them to freely diffuse into the field of view. We observed many dynamic binding interactions within each assay chamber, in parallel, using our EMCCD camera. As illustrated in Figure 3, the time-resolved

dx.doi.org/10.1021/ac4004453 | Anal. Chem. XXXX, XXX, XXX−XXX

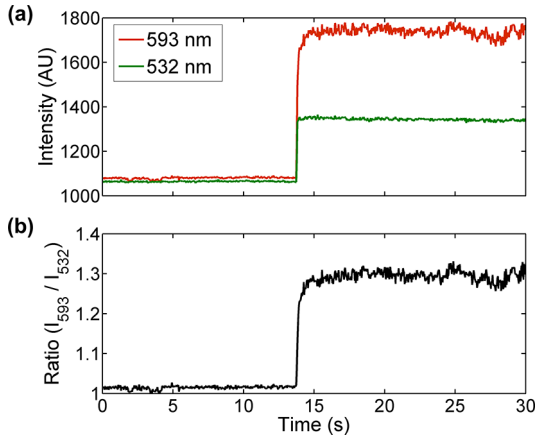

Figure 3. Time-resolved binding between GNPs. Time-resolved binding events between a freely diffusing neutravidin-GNP and a surface-bound biotin-GNP are recorded with 38 ms time exposure (26 Hz). We observed binding events between GNPs in all assay chambers. The representative time record of a single GNP interaction shows (a) the time-dependent scattering signals from the 593 nm (red) and 532 nm (green) channels and (b) the change in intensity ratio between the two channels (I_{593}/I_{532}). Whereas dynamic binding detection only requires measurement of the total intensity, the intensity ratio offers the ability to quantify further details, such as orientation of the particle pair by polarization sensitivity or interparticle separations.

intensity traces are consistent with a specific binding interaction between two GNPs. The total intensity more than doubles with intensity increases in both the 532 and 593 nm channels, indicating that a second scattering particle is within the diffraction-limited region. The scattering intensity ratio also increases, as is expected when two GNPs bind and preferentially scatter longer wavelengths. This change in intensity ratio confirms that the observed interaction involves plasmonic coupling, and thus, we conclude that two GNPs are brought into close proximity in an interaction that is mediated by binding between neutravidin and biotin. After the initial ratio increase, the intensity ratio remains unchanged, indicating that the event is a stable binding event.

The initial intensity ratio from the surface-bound biotin-GNP is 0.938 ± 0.14. When we limited our analysis to only binding events in which the initial intensity ratio is consistent with monomeric GNPs, the intensity ratio increases by a factor of 1.5 to 2, consistent with our previous observations. Further, we observe that RAMEDI is sensitive to detecting binding between nonideal GNPs, such as larger aggregates, anisotropic particles, or even multiple particles, though the absolute values of the initial and final intensity ratios are varied (see Supporting Information). From the time-resolved binding events using RAMEDI, we demonstrate an observable bandwidth of >25 Hz with a signal-to-background ratio better than 100. As previously noted, however, RAMEDI is extendable to faster time scales.

The signal-to-noise ratio in the ratiometric analysis technique is important for future applications of RAMEDI to metrology and as an alternative to FRET. Ultimately, the ability to discriminate substates or substeps for a given dynamic process is directly related to the signal change corresponding to a single step and inversely proportional to the noise in the signal.[29] Following the methodology of Ueno et al.,[26] we determined the signal-to-noise ratio for the RAMEDI technique to be 25 for changes in the intensity ratio accompanying dynamic binding interactions between biotin and neutravidin. Simulations that vary both the number of steps in a record and the dwell times between steps specify with ±10% precision that a signal-to-noise ratio of 4 is adequate to detect stepwise transitions between intermediate states.[29,30] Using this criterion, the signal-to-noise ratio for the RAMEDI technique is sufficient to discriminate at least six equally spaced intermediate states within a dynamic, molecular interaction resulting in changes of the interparticle separation over the detectable range. This consideration suggests RAMEDI can be extended beyond a simple, yet highly sensitive, binding detection method and may be used to capture the substates within dynamic processes.

Plasmonic Coupling Polarization Sensitivity Detection Using RAMEDI. Plasmonic coupling between GNPs is dependent on the alignment of the dimer axis relative to the linear polarization of the illumination.[6,14,15,19,31] When the dimer axis is aligned with the electric field, the coupling is maximized. Conversely, there is little or no enhancement when the polarization is orthogonal to the dimer axis. Conventional darkfield illumination using a condenser lens is problematic for detecting polarization dependent scattering because it illuminates the sample using a conical annulus with high numerical aperture. It has been recently reported that it is not possible to determine the unique three-dimensional orientation of a GNP pair over the full range of possible dimer axis alignments using a darkfield condenser.[32] Additionally, not using polarization filters with the darkfield illumination averages the overall scattering signal over all polarizations, which reduces the scattering response from the particles. Using the RAMEDI technique removes many of the limitations that accompany use of a darkfield condenser.

RAMEDI propagates the light along the glass slide of the sample, parallel to the glass surface. To quantify the sensitivity of RAMEDI to polarization, we used a polarizing beamsplitter to selectively illuminate GNPs with two wavelengths of monochromatic, linearly polarized light. Before introducing the neutravidin-GNPs, we imaged surface-bound biotin-GNPs while illuminating with the polarized light and then calculated the initial intensity ratio between the two wavelengths of light scattered from each GNP. We repeated this intensity ratio measurement after rotating the polarizing beamsplitter and selectively illuminating the sample with an orthogonal polarization of light. Subsequently, neutravidin-GNPs were introduced into the sample chamber and incubated for 15 min, and the intensity ratios were again measured from images recorded under both polarizations.

As expected, binding of neutravidin-GNPs to biotin-GNPs illuminated with the two orthogonal polarizations were made evident by an increase in both the total intensity and the I_{593}/I_{532} intensity ratio. After binding, the change in the intensity ratio was dependent on the linear polarization of the illumination, as demonstrated in Figure 4. Surface-bound GNPs not bound by neutravidin-GNPs again served as internal controls to establish that the observed polarization sensitivity in the binding interactions arises from plasmonic coupling. Interestingly, we were able to observe the plasmonic signature of a bound pair of GNPs with the dimer axis whose 2D projection is aligned with the 0° polarization angle (see Figure 4e, particle 2; note that, at 90°, no plasmonic enhancement is observed, as expected if the projection of the dimer axis is orthogonal to the polarization). From this observation, we calculate a polarization sensitivity of ∼20, a value that is consistent with previous theoretical and experimental polar-

dx.doi.org/10.1021/ac4004453 | Anal. Chem. XXXX, XXX, XXX−XXX

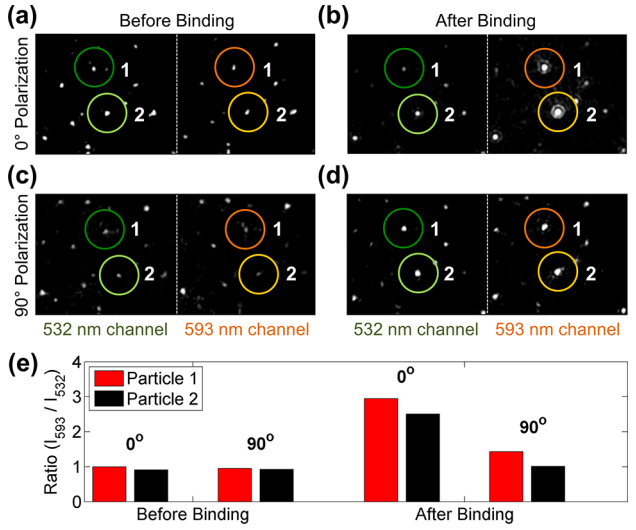

Figure 4. Polarization sensitivity of the plasmonic coupling response from the particle pair. Images were collected from the same field of view under illumination from two orthogonally polarized sources, both before and after a 15 min incubation with neutravidin-GNPs. (a, c) Before binding of a second GNP, the surface-bound biotin-GNPs are observed under two orthogonal polarization states: (a) 0° and (c) 90°. (b, d) After a 15 min incubation, images were again collected from the same field of view using the two previous polarization orientations: (b) 0° and (d) 90°. A polarization dependent change in the I_{593}/I_{532} intensity ratio after binding of a second GNP reveals the sensitivity of the alignment of the GNP dimer axis to the polarization of the illumination, as indicated in (e). Note that particle 2 exhibits minimal plasmonic enhancement at 90°, but a 2.5-fold increase in the ratio at 0° after binding, indicating that the dimer axis is nearly aligned with that polarization axis.

ization sensitivity measurements for GNPs.[22,33] The polarization sensitivity of the RAMEDI technique makes it in principle possible to determine the in-plane orientation of the GNP dimer axis. To fully define the three-dimensional angular orientation of the GNP dimer pair, a second illumination source propagating in a direction that is perpendicular to the first is required, similar to the illumination method described by Xiao et al.[32]

CONCLUSIONS

Motivated by the efforts of Sonnichsen et al. to establish that plasmonic coupling between metallic nanoparticles could be a viable alternative method to FRET,[11,12] we sought to overcome the technical limitations with prior illumination methods that have thus far limited the temporal resolution of the molecular ruler technique. We developed a novel monochromatic excitation technique with ratiometric analysis of the scattering from GNPs. As a proof-of-principle demonstration, we used RAMEDI to observe, with high temporal resolution, the plasmonic coupling response resulting from the binding of a neutravidin-GNP to a surface-bound biotin-GNP. We report the detection of the plasmonic coupling between two GNPs with greater than 25 Hz bandwidth, limited only by the speed of our detector. At this bandwidth, individual GNPs were imaged with a signal-to-noise ratio better than 100 and greater than 20 at 200 Hz. Our observations demonstrate that RAMEDI is, in principle, capable of achieving the microsecond time resolution demonstrated in objective-type darkfield illuminations schemes, where alternate detectors with higher temporal resolution are used.[26,34] We calculated the intensity ratio from the scattered light by the GNPs from two sampling wavelengths and found good agreement with published theoretical simulations. Upon binding by a second GNP, the intensity ratio more than doubles and yields an observable change with a high signal-to-noise ratio. Finally, we established that RAMEDI is sensitive to the orientation of the dimer axis of the GNP pair, exploiting the known dependence of plasmonic coupling to the polarization state of the incident excitation.

While RAMEDI improves upon the previous applications of plasmonic coupling between metallic nanoparticles, several technical challenges remain. For example, future implementations of the RAMEDI technique seeking to measure the distance between two nanoparticles with high precision (as in single-molecule FRET) must recognize that the measurement precision will be tightly coupled to the size and shape distributions of the GNPs. Any heterogeneity in the GNP populations will have direct implications on the observed plasmonic response, thus contributing to uncertainty in the measured distance and polarization dependence. Therefore, the scattering intensity ratio measured using RAMEDI will need to be quantified as a function of the homogeneity of particle geometry in a given GNP solution. Additionally, future implementations of RAMEDI will require careful selection of the sampling wavelengths to maximize the sensitivity of the measurement for specific particle separations that are anticipated to occur between the GNPs during the dynamic interaction (see Supporting Information for details).

However, despite these technical challenges, RAMEDI offers many advantages over other techniques, including significantly enhanced signal strength and photostability. In addition, RAMEDI is envisioned to be a single-molecule technique with superior spatial and temporal resolution over conventional fluorescence-based methods. The observations reported here clearly establish that the ratiometric plasmonic detection technique we have developed can not only be applied to observing dynamic behavior between an enzyme and its substrate but also be used to discriminate multiple interparticle distances and/or orientations. In future applications where multiple states need to be identified, the low-noise signal that we observed during the binding assay is theoretically expected to resolve six substates, establishing the possibility of multistep detection.[29,30] Indeed, as one possible application of this assay, we have successfully verified that multiple states can be observed between a free GNP in solution that is conjugated to bacteriophage T7 RNA polymerase and a fixed GNP coated with DNA encoding the polymerase's promoter sequence (see Supporting Information). While yet to be fully interpreted, the preliminary T7 RNA polymerase binding observation establishes that multiple, dynamic states can be observed using this method and serves to highlight the potential of this technique to be applied as a sensitive single-molecule technique akin to FRET.

We present an evanescent darkfield illumination technique with broad and diverse use for systems involving plasmonic nanoparticles, including single-molecule biophysics, biotechnology and biosensing, and plasmonics. RAMEDI is ideal for gold nanoparticle tracking, having all of the advantages of objective-type darkfield illumination while preserving image quality.[26,34−36] The use of evanescent darkfield illumination and ratiometric detection can improve the sensitivity of molecular binding assays (akin to Nusz et al.[18]) and enables enhanced illumination and detection of plasmonic nanostructures.[37−39]

dx.doi.org/10.1021/ac4004453 | Anal. Chem. XXXX, XXX, XXX−XXX

Taken together, the data presented herein demonstrate that RAMEDI addresses many of the technical issues currently limiting the broader use of plasmonic coupling between gold nanoparticles[11,12,16,22−24,27] as a superior alternative to FRET-based characterization of real-time, nanometer-scale molecular activity.

■ ASSOCIATED CONTENT

Supporting Information

Additional figures and information. This material is available free of charge via the Internet at http://pubs.acs.org.

■ AUTHOR INFORMATION

Corresponding Author

*D.M.W.: phone, (734) 277-7947; fax, (404) 727-0873; e-mail, dianemariewiener@gmail.com. T.A.L.: phone, (734) 730-5983; fax, (510) 643-4500; e-mail, talionberger@gmail.com.

Present Addresses

[†]Diane M. Wiener: Department of Physics, Emory University, Atlanta, GA 30322, USA.

[¶]Troy A. Lionberger: Howard Hughes Medical Institute and Jason L. Choy Laboratory of Single-Molecule Biophysics, Department of Physics, University of California, Berkeley, CA 94720, USA.

Author Contributions

The manuscript was written through contributions of all authors. All authors have given approval to the final version of the manuscript.

Notes

The authors declare no competing financial interest.

■ ACKNOWLEDGMENTS

This work was supported by the National Science Foundation Graduate Research Fellowship (D.M.W. and T.A.L.) and the National Defense Science and Engineering Graduate Fellowship (D.M.W. and T.A.L.). We thank N. Perkins and K. Kurabayashi for support and helpful discussions. We also thank E. Meyhöfer for funding and support in the early phases of this work.

■ REFERENCES

(1) Ha, T.; Enderle, T.; Ogletree, D. F.; Chemla, D. S.; Selvin, P. R.; Weiss, S. *Proc. Natl. Acad. Sci. U. S. A.* **1996**, *93*, 6264−6268.

(2) Donnert, G.; Eggeling, C.; Hell, S. W. *Nat. Methods* **2007**, *4*, 81−86.

(3) Yguerabide, J.; Yguerabide, E. *Anal. Biochem.* **1998**, *262*, 137−156.

(4) Kreibig, U.; Vollmer, M. *Optical properties of metal clusters*; Springer: New York, 1995; p 532.

(5) Kelly, K. L.; Coronado, E.; Zhao, L. L.; Schatz, G. C. *J. Phys. Chem. B* **2003**, *107*, 668−677.

(6) Jain, P. K.; Lee, K. S.; El-Sayed, I. H.; El-Sayed, M. A. *J. Phys. Chem. B* **2006**, *110*, 7238−7248.

(7) Jain, P. K.; Huang, X.; El-Sayed, I. H.; El-Sayed, M. A. *Acc. Chem. Res.* **2008**, *41*, 1578−1586.

(8) Sepúlveda, B.; Angelomé, P. C.; Lechuga, L. M.; Liz-Marzán, L. M.; Sepulveda, B.; Angelome, P. C.; Liz-Marzan, L. M. *Nano Today* **2009**, *4*, 244−251.

(9) Oldenburg, S. J.; Averitt, R. . D.; Westcott, S. . L.; Halas, N. J. *Chem. Phys. Lett.* **1998**, *288*, 243−247.

(10) El-Sayed, M. A. *Acc. Chem. Res.* **2001**, *34*, 257−264.

(11) Reinhard, B. M.; Siu, M.; Agarwal, H.; Alivisatos, A. P.; Liphardt, J. *Nano Lett.* **2005**, *5*, 2246−2252.

(12) Sönnichsen, C.; Reinhard, B. M.; Liphardt, J.; Alivisatos, A. P.; Sonnichsen, C. *Nat. Biotechnol.* **2005**, *23*, 741−745.

(13) Liu, G. L.; Yin, Y.; Kunchakarra, S.; Mukherjee, B.; Gerion, D.; Jett, S. D.; Bear, D. G.; Gray, J. W.; Alivisatos, A. P.; Lee, L. P.; Chen, F. F. *Nat. Nanotechnol.* **2006**, *1*, 47−52.

(14) Rechberger, W.; Hohenau, A.; Leitner, A.; Krenn, J. R. R.; Lamprecht, B.; Aussenegg, F. R. R. *Opt. Commun.* **2003**, *220*, 137−141.

(15) Su, K.-H. H.; Wei, Q.-H. H.; Zhang, X.; Mock, J. J.; Smith, D. R.; Schultz, S. *Nano Lett.* **2003**, *3*, 1087−1090.

(16) Reinhard, B. M.; Sheikholeslami, S.; Mastroianni, A.; Alivisatos, A. P.; Liphardt, J. *Proc. Natl. Acad. Sci. U. S. A.* **2007**, *104*, 2667−2672.

(17) Raschke, G.; Kowarik, S.; Franzl, T.; Sönnichsen, C.; Klar, T. A.; Feldmann, J.; Nichtl, A.; Kürzinger, K.; Sonnichsen, C.; Kurzinger, K. *Nano Lett.* **2003**, *3*, 935−938.

(18) Nusz, G. J.; Marinakos, S. M.; Curry, A. C.; Dahlin, A.; Hook, F.; Wax, A.; Chilkoti, A.; Höök, F. *Anal. Chem.* **2008**, *80*, 984−989.

(19) Jain, P. K.; Huang, W. Y.; El-Sayed, M. A. *Nano Lett.* **2007**, *7*, 2080−2088.

(20) Jain, P. K.; El-Sayed, M. A. *Nano Lett.* **2008**, *8*, 4347−4352.

(21) Novo, C.; Funston, A. M. M.; Pastoriza-Santos, I.; Liz-Marzan, L. M. M.; Mulvaney, P. *J. Phys. Chem. C* **2008**, *112*, 3−7.

(22) Wang, H. Y.; Reinhard, B. M. *J. Phys. Chem. C, Nanomater. Interfaces* **2009**, *113*, 11215−11222.

(23) Rong, G.; Wang, H.; Reinhard, B. M. *Nano Lett.* **2010**, *10*, 230−238.

(24) Reinhard, B. M.; Yassif, J. M.; Vach, P.; Liphardt, J. *Methods Enzymology* **2010**, *475*, 175−198.

(25) Braslavsky, I.; Amit, R.; Ali, B. M. J.; Gileadi, O.; Oppenheim, A.; Stavans, J.; Jaffar Ali, B. M. *Appl. Opt.* **2001**, *40*, 5650.

(26) Ueno, H.; Nishikawa, S.; Iino, R.; Tabata, K. V; Sakakihara, S.; Yanagida, T.; Noji, H. *Biophys. J.* **2010**, *98*, 2014−2023.

(27) Rong, G.; Wang, H.; Skewis, L. R.; Reinhard, B. M. *Nano Lett.* **2008**, *8*, 3386−3393.

(28) Jung, L. S.; Nelson, K. E.; Stayton, P. S.; Campbell, C. T. *Langmuir* **2000**, *16*, 9421−9432.

(29) Moffitt, J. R.; Chemla, Y. R.; Smith, S. B.; Bustamante, C. *Annu. Rev. Biochem.* **2008**, *77*, 205−228.

(30) Wallin, A. E.; Salmi, A.; Tumay, R. *Biophys. J.* **2007**, *93*, 795−805.

(31) Link, S.; Wang, Z.; El-Sayed, M. *J. Phys. Chem.* **1999**, *103*, 3529−3533.

(32) Xiao, L. H.; Qiao, Y. X.; He, Y.; Yeung, E. S. *J. Am. Chem. Soc.* **2011**, *133*, 10638−10645.

(33) Grecco, H. E.; Martinez, O. E. *Opt. Express* **2006**, *14*, 8716−8721.

(34) Nan, X.; Sims, P. A.; Xie, X. S. *ChemPhysChem* **2008**, *9*, 707−712.

(35) Dunn, A. R.; Spudich, J. A. *Nat. Struct. Mol. Biol.* **2007**, *14*, 246−248.

(36) Grecco, H. E.; Martínez, O. E. *Pap. Phys.* **2011**, 2.

(37) Bath, J.; Turberfield, A. J. *Nat. Nanotechnol.* **2007**, *2*, 275−284.

(38) Park, S. Y.; Lytton-Jean, A. K. R.; Lee, B.; Weigand, S.; Schatz, G. C.; Mirkin, C. A. *Nature* **2008**, *451*, 553−556.

(39) Tan, S. J. J.; Campolongo, M. J. J.; Luo, D.; Cheng, W. L. *Nat. Nanotechnol.* **2011**, *6*, 268−276.